sciendo

DOI 10.2478/ama-2024-0017

acta mechanica et automatica, vol.18 no.1 (2024)

COMPUTER SIMULATION OF HEAT AND MASS TRANSFER EFFECTS ON NANOFLUID FLOW OF BLOOD THROUGH AN INCLINED STENOSED ARTERY WITH HALL EFFECT

Nidhish Kumar MISHRA*

*Department of Basic Science, College of Science and Theoretical Studies, Saudi Electronic University, Riyadh 11673, Saudi Arabia

n.kumar@seu.edu.sa

received 5 May 2023, revised 18 July 2023, accepted 19 July 2023

Abstract: The present study deals with the analysis of heat and mass transfer for nanofluid flow of blood through an inclined stenosed artery under the influence of the Hall effect. The effects of hematocrit-dependent viscosity, Joule heating, chemical reaction and viscous dissipation are taken into account in the governing equations of the physical model. Non-dimensional differential equations are solved using the finite difference method, by taking into account the no-slip boundary condition. The effects of different thermophysical parameters on the velocity, temperature, concentration, shear stress coefficient and Nusselt and Sherwood numbers of nano-biofluids are exhaustively discussed and analysed through graphs. With an increase in stenosis height, shear stress, the Nusselt number and the Sherwood number are computed, and the impacts of each are examined for different physical parameters. To better understand the numerous phenomena that arise in the artery when nanofluid is present, the data are displayed graphically and physically described. It is observed that as the Hartman number and Hall parameter increase, the velocity drops. This is as a result of the Lorentz force that the applied magnetic field has generated. Blood flow in the arteries is resisted by the Lorentz force. This study advances the knowledge of stenosis and other defects' non-surgical treatment options and helps reduce post-operative consequences. Moreover, ongoing research holds promise in the biomedical field, specifically in magnetic resonance angiography (MRA), an imaging method for artery examination and anomaly detection.

Key words: Chemical reaction, Hall effect, Joule heating, Nanofluid, Variable viscosity.

1. INTRODUCTION

Blood is a biological fluid that nourishes and supplies the cells with oxygen. Additionally, it facilitates the removal of waste from cells. Since the blood in the artery circulates throughout the entire body, it is a crucial component. The presence of stenosis reduces the blood flow through an artery. The blood vessel becomes narrowed when there is stenosis [1]. This syndrome is brought on by lipid buildup in the artery wall or by pathological alterations in the tissue structure [2]. Additionally, it is brought on by the lumen's accumulation of cholesterol, fatty substances, calcium, cellular debris and fibrin [3]. Changes in the artery's pressure and flow are brought on by the deposition in the arterial wall. Heart failure results from the diminished blood supply, which has major circulation consequences [4]. Applications for the study of blood flow in arteries can be found in both engineering and medicine [5]. Additionally, it aids in the treatment of artery stenosis and the design of cardiovascular devices. Cells suspended in plasma make up blood. The viscosity of plasma and blood cells determines the viscosity of blood. Water quantity and plasma proteins affect plasma viscosity [6]. Red blood cells, which predominate over white blood cells in terms of quantity, determine the viscosity of blood; 45% of the total volume of blood is made up of red blood cells [7]. Hematocrit, a volume proportion used to express red blood cells in the blood. Hematocrit and temperature have a significant impact on blood viscosity. Blood viscosity is significantly influenced by hematocrit [8]. Viscosity increases dramatically and generates more flow resistance as hematocrit levels rise [9]. The oxygen supply is reduced as a result [10]. Recently, Asgar et al. [11] investigated electro-osmotically driven generalised Newtonian blood flow in a divergent micro-channel. Therefore, it is important to comprehend how viscosity changes with hematocrit.

As red blood cells include the iron component haemoglobin, blood is thought to carry electricity [12]. Therefore, the magneto hydrodynamics (MHD) principle can be used to investigate how a magnetic field affects arterial blood flow. The Lorentz force will oppose the motion of the blood when an external field is introduced. Treatment for circulatory diseases is aided by this. This supports one of the medication delivery strategies, magnetic drug targeting [13]. Due to its non-invasiveness, excellent targeting efficiencies and less harmful side effects on healthy cells and tissues, magnetic drug targeting is effective [14]. Sharma et al. [15] focused on the core and plasma regions when they studied MHD two-phase blood flow. They found that although the presence of heat reduces the likelihood of atherosclerosis, wall permeability and curvature increase it. Kumawat et al. [16] have examined the entropy formation on MHD two-phase blood flow with heat and mass transfer. Additionally, heat is produced as a result of an electric current's conduction through a conducting fluid. Joule heating is the name given to the heat that is created. Joule first law explains how current and heat are related. Studying this phenomenon contributes to a better comprehension of the rise in arterial temperature. A conducting fluid also experiences the Hall effect. The Lorentz force that results from the application of an external field causes charges to move in the opposite direction of the flow, resisting the flow. Because a magnetic field can control blood flow, it is employed as a blood pump to carry out cardiac surgeries in stenosed conditions [7]. When an external

magnetic field is used during magnetic resonance imaging, the impact of the magnetic field on blood flow via arteries is significant. Numerous studies [17–21] have examined the flow issues of viscous incompressible fluid via various geometries with the Hall effect. In the study by Ramzan et al. [22], investigation of the 3D nanofluid flow took into account Hall and ion slip effects, Arrhenius activation energy and Cattaneo-Christov heat flux. Using silver and aluminium oxide nanoparticles as the base fluid, Das et al. [23] recently employed the Casson fluid model to demonstrate the rheology of blood and investigate Hall and ion slip effects. Raja et al. [24] have explored the boundary layer flow problem in the presence of heat radiation and Hall current approaching the stretched sheet. They numerically deployed their models using the Adomian decomposition method. Das et al. [25], Kada et al. [26] and Asgar et al. [27] demonstrated the MHD movement of a three-dimensional Carreau-nanofluid under the effect of different physical situations. The results of this experiment demonstrate that the heat generating parameter raised the nanofluid's temperature. When radiation therapy is used, the impact of the radiation parameter must be taken into account. When a radioactive stent is inserted into a stenosed artery to control blood flow, the arteries are also exposed to radiation [28]. The effects of radiation on stenosis are better understood by study of the radiation parameter. Thermal radiation impact on an unsteady MHD nanofluid flow for Newtonian and non-Newtonian fluid has been discussed by Bejawada and Nandeppanavar [29], Jamshed et al. [30] and Reddy and Goud [31]. Sharma et al. [32, 33] analysed an unsteady MHD free and forced convection for a heat-generating fluid with and without thermal radiation and chemical reaction. In a compliant wall channel with thermal radiation and heat generation, Makinde et al. [34] analysed the impact of MHD and heat transfer on the peristaltic flow of Walters-B fluid. Mishra [35] has recently explored the radiation influence on thermal and mass diffusion MHD blood flow through a tapered porous stenosed artery. Arteriovenous stenosis is treated with nanofluids. Colloidal suspensions of nanoparticles in a base fluid are known as nanofluids [36]. Typically, base fluids such water, ethylene glycol, oil and biofluids are used to suspend nanoparticles of Ag, Cu, Al2O3 and TiO2 [37]. Compared to base fluids, nanofluids have improved thermal conductivity [1]. Techniques for treating vascular stenosis are developed with the use of nanoparticle analysis of blood flow in stenosed arteries. To investigate the impact of hybrid nanoparticles (Au-Al2O3) on blood that is subject to temperature-dependent viscosity, Gandhi et al. [38] used the bell-shaped artery. Sharma et al. [39] have investigated the MHD slip flow with tapered multiple-stenosis artery using an entropy analysis. Blood-carrying vessels that are horizontal or vertical were taken into account in all the investigations listed before. Analysis of low Reynolds number flow generated in complex wavy surfaces has been discussed by Asgar et al. [40–43].

Chemical reactions in fluid flow have utility in energy production (combustion), pollution control (scrubbing) and industrial processes (chemical synthesis). They play a vital role in transforming substances, generating energy and altering fluid properties, impacting various sectors and contributing to both environmental and industrial advancements. The effect of chemical reaction and flow with the MHD effect on heat and mass transfer of fluid flow through different geometries has been analysed previously [44–48]. It is commonly known, however, that many ducts in physiological systems are inclined to the axis, rather than being horizontal or vertical. The inclined arterial blood flow with magnetic field was discussed by Sharma et al. [49] and Srinivasulu and Goud [50]. Nevertheless, the examination of blood flow characteristics through an inclined artery with changing viscosity is still missing from the literature.

The influence of nanoparticles on blood flow in an inclined porous artery is examined in the current research by taking into account viscosity varying with hematocrit, viscous dissipation, chemical reaction, radiation, Joule heating and the Hall effect. A comprehensive survey of the literature revealed that no communication has been addressed to discuss the computational analysis on the blood flow through an inclined artery under a strong magnetic field. By factoring in viscosity change with hematocrit, viscous dissipation, radiation, Joule heating and the Hall effect, this study analyses the impact of these physical parameters on blood flow in an inclined porous artery.

By adding the aforementioned effects, the governing equations for mass, momentum, energy and concentration are framed. The Thomas algorithm is used to solve the resulting discretised non-dimensionalised equations using the finite difference approach. Analysis is carried out on how these parameters affect temperature, concentration and velocity profiles. Additionally, the Nusselt number, shear stress and the Sherwood number are computed. Along the stenosis height, the impacts of several parameters on the shear stress, the Sherwood number and the Nusselt number profile are investigated.

The novelty and objectivity of this investigation are concentrated on the following items:

- The combined effects of viscous dissipation, radiation, Joule heating and the Hall effect on the hemodynamic flow are examined.
- The effect of hematocrit-dependent viscosity on the blood flow through the stenosed artery is analysed.
- FDM analysis is performed to investigate the skin friction coefficient and the local Nusselt number with different physical parameters.

2. MATHEMATICAL FORMULATION OF THE MODEL

Consider a viscous, incompressible nanofluid MHD flow of blood through an inclined porous artery with variable viscosity and stenosis under the effect of Hall current, Joule heating and viscous dissipation. Joshi and Srivatsava [51, 52] characterised the geometrical representation of the arterial wall under the mild stenosed condition as,

$$\frac{R(z)}{R_0} = \begin{Bmatrix} 1 - \frac{2\delta}{R_0 L_0}(z-d) & d < z \leq d + \frac{L_0}{2} \\ 1 - \frac{\delta}{2R_0}\left(1 + cos\frac{2\pi}{L_0}\left(z - d - \frac{L_0}{2}\right)\right) & d + \frac{L_0}{2} < z \leq d + L_0 \\ 1 & otherwise \end{Bmatrix} \tag{2.1}$$

The physical model of the problem is depicted in Fig. 1. It is assumed that fluid is flowing in the z-direction. Also, R (z), Ro, d, Lo and δ are the radius of the artery in the obstructed region, radius of the normal artery, and location, length and height of stenosis, respectively.

The flow of the fluid is modelled by making the following assumptions:

- An unsteady, incompressible, viscous electrical

conducting MHD fluid with viscous dissipation, Joule heating, Hall effect and thermal radiation is under consideration.
- The flow is assumed to be independent of θ direction due to axi-symmetry condition of the artery.
- The magnetic Reynold number is considered very small (Re≪1) so that the induced magnetic field can be neglected as compared to the applied magnetic field.
- We assumed the blood to be a Newtonian fluid flowing through the composite stenosis.

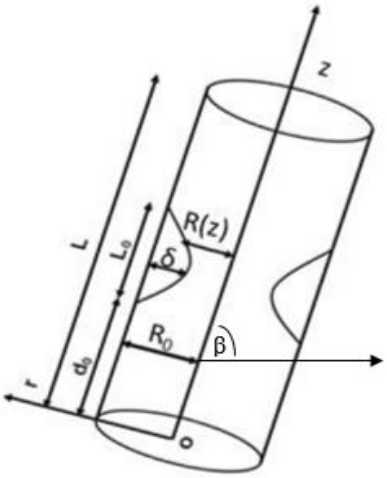

Fig.1. Schematic diagram of an inclined artery

The governing equations for the considered mathematical model with appropriate assumptions can be written as follows:

Continuity equation:

$$\frac{1}{r}\frac{\partial(rv)}{\partial r}+\frac{\partial u}{\partial z}=0 \tag{2.2}$$

Momentum equation (r-direction):

$$\rho_f\left(v\frac{\partial v}{\partial r}+u\frac{\partial v}{\partial z}\right)=-\frac{\partial p}{\partial r}-\left[\frac{1}{r}\frac{\partial(r\tau_{rr})}{\partial r}+\frac{\partial\tau_{zr}}{\partial z}+\frac{\tau_{\theta\theta}}{r}\right]-\frac{\sigma\widetilde{B^2}}{1+Be^2}\,(v+Be\,u) \tag{2.3}$$

Momentum equation (z-direction):

$$\rho_f\left(v\frac{\partial u}{\partial r}+u\frac{\partial u}{\partial z}\right)=-\frac{\partial p}{\partial z}-\left[\frac{1}{r}\frac{\partial(r\tau_{rz})}{\partial r}+\frac{\partial\tau_{zz}}{\partial z}\right]$$
$$-\mu(T)\frac{u}{k_1}+\rho_f g cos\beta\alpha_T(T-T_0)\;+\rho_f g cos\beta\alpha_c(C-C_0)+\frac{\mu(r)u}{k_1}\;-\frac{\sigma\widetilde{B^2}}{1+Be^2}\,(u+Be\,v) \tag{2.4}$$

Energy equation:

$$(\rho C_p)_f\left(v\frac{\partial T}{\partial r}+u\frac{\partial T}{\partial z}\right)=k_T\left[\frac{\partial^2T}{\partial r^2}+\frac{1}{r}\frac{\partial T}{\partial r}+\frac{\partial^2T}{\partial z^2}\right]-\frac{1}{r}\frac{\partial(rq_r)}{\partial r}+\left\{\frac{\sigma\widetilde{B^2}}{1+Be^2}\,(u^2+v^2\right\}+\mu(r)\left(\frac{\partial u}{\partial r}\right)^2 \tag{2.5}$$

Concentration equation:

$$\left(v\frac{\partial C}{\partial r}+u\frac{\partial C}{\partial z}\right)=D_m\left[\frac{\partial^2C}{\partial r^2}+\frac{1}{r}\frac{\partial C}{\partial r}+\frac{\partial^2C}{\partial z^2}\right]\;-K_r(-C_0) \tag{2.6}$$

Corresponding boundary conditions are as follows:

$$\frac{\partial u}{\partial r}=0,\qquad \frac{\partial T}{\partial r}=0,\qquad \frac{\partial C}{\partial r}=0 \tag{2.7}$$

at $r=R(z)/R_0$

$$u=0,\qquad T=T_0,\qquad C=C_0 \tag{2.8}$$

The radioactive heat flux is defined as follows:

$$q_r=\frac{-4\sigma_s}{3k_e}\frac{\partial T^4}{\partial r}.$$

where ke is the absorption coefficient and σ_s is the Stefan–Boltzmann constant.

For realistic behaviour, viscosity of blood is considered a variable (a function of radius), and $\tilde{\mu}(r)$ is defined by Einstein formula [53],

$$\tilde{\mu}(r)=\mu_0[1+\tilde{\lambda}h(r].$$

where $\tilde{\lambda}$ is a constant (2.5 for blood) and h(r) is for hematocrit, which is defined by Lih [54],

$$h(r)=H\left[1-\left(\frac{r}{R_0}\right)^m\right]$$

H is the hematocrit at the centre and m (≥ 2) determines the shape of velocity profile of the blood.

The components of the Hall parameter [37] are as follows:

$$J_X=\frac{\tilde{B}\sigma}{1+Be^2}(uBe-v),J_z=\frac{\tilde{B}\sigma}{1+Be^2}(u+vBe),$$

where B is the magnetic induction vector, Jx and Jz are the current density vectors, σ the electrical conductivity, te is the electrical collision time, Be = te ωe is the Hall parameter and ωe is the electron frequency.

Dimensionless parameters used in the equations are as follows:

$$\bar{r}=\frac{r}{R_0},\quad \bar{p}=\frac{R_0^2}{UL_0\mu_f}p,\quad \bar{z}=\frac{z}{L_0},\quad \bar{\mu}=\frac{\mu}{\mu_f},$$

$$\bar{R}=\frac{R}{R_0},\qquad K_1=\frac{k_1}{R_0},R=\frac{k_ek}{4R\sigma_sT_0^3}$$

$$\bar{u}=\frac{u}{U},\;\; B_r=\frac{U^2\mu}{kT_0},M^2=\frac{\sigma B_0^2R_0^2}{\mu_f},\quad \sigma=\frac{C-C_0}{C_0},$$

$$K=\frac{K_rR_0^2\tau_0C_0}{\alpha},\;\; Gr=\frac{g\alpha_TR_0^2T_0\rho_f}{U\mu_f},\;\; P_r=\frac{\mu_fc_{pf}}{k},$$

$$\bar{v}=\frac{L_0}{\delta U}v,\;\; \bar{d}=\frac{d}{L_0},\quad Cr=\frac{g\alpha_CR_0^2C_0\rho_f}{U\mu_f},\quad \bar{\delta}=\frac{\delta}{R_0},$$
$$\theta=\frac{T-T_0}{T_0},\quad \alpha=\frac{k}{(\rho c_p)_f}$$

where k1 is the porosity parameter, Br is the Brinkman number, Gr is the Grashof number, Cr is the modified Grashof number, M is the Hartmann number, K is a reaction rate constant.

The governing equations are simplified to dimensionless forms by substituting the aforementioned dimensionless parameters and applying the additional conditions:

$\epsilon=\frac{R_0}{L_0}\cong O(1)$ for the case of mild stenosis $\left(\frac{\delta}{R_0}\ll 1\right)$.

The governing equations in non-dimensional form after dropping the dashes can be written as follows:

$$\frac{\partial \mathrm{p}}{\partial \mathrm{r}} = 0 \tag{2.9}$$

$$\frac{\partial \mathrm{p}}{\partial z} = \frac{1}{\mathrm{r}}\frac{\partial}{\partial \mathrm{r}}\left(\mathrm{r}\mu(\mathrm{r})\frac{\partial \mathrm{u}}{\partial \mathrm{r}}\right) - \left(\frac{\mu(\mathrm{r})}{\mathrm{K}_1}\right)\mathrm{u} + \mathrm{Gr}\theta\cos\beta + \mathrm{Cr}\sigma\ \cos\beta - \mathrm{u}\ \frac{M^2}{1+Be^2} \tag{2.10}$$

$$\left(1+\frac{4}{3R}\right)\left(\frac{1}{\mathrm{r}}\frac{\partial}{\partial \mathrm{r}}\left(\mathrm{r}\frac{\partial \boldsymbol{\theta}}{\partial \mathrm{r}}\right)\right) + \mathrm{Br}\mu(\mathrm{r})\left(\frac{\partial \mathrm{u}}{\partial \mathrm{r}}\right)^2 + \frac{\mathrm{M}^2\mathrm{u}^2 Br}{1+Be^2} = 0 \tag{2.11}$$

$$\left(\frac{1}{\mathrm{r}}\frac{\partial}{\partial \mathrm{r}}\left(\mathrm{r}\frac{\partial \boldsymbol{\sigma}}{\partial \mathrm{r}}\right)\right) - \boldsymbol{\sigma}\mathrm{K} = 0 \tag{2.12}$$

The dimensionless form of corresponding boundary conditions is as follows:

at $\mathrm{r} = 0$

$$\frac{\partial \mathrm{u}}{\partial \mathrm{r}} = 0, \qquad \frac{\partial \boldsymbol{\theta}}{\partial \mathrm{r}} = 0, \qquad \frac{\partial \boldsymbol{\sigma}}{\partial \mathrm{r}} = 0 \tag{2.13}$$

at $\mathrm{r} = R(z)$

$$\mathrm{u} = 0, \qquad \theta = 0 \qquad \sigma = 0 \tag{2.14}$$

The mathematical expression of the geometry of the arterial wall in the dimensionless form is as follows:

$$R(z) = \begin{Bmatrix} 1 - 2\delta(z-d) & d < z \leq d + \frac{1}{2} \\ 1 - \frac{\delta}{2}\left(\cos 2\pi\left(\frac{1+z-d}{-\frac{1}{2}}\right)\right) & d + \frac{1}{2} < z \leq d + 1 \\ 1 & otherwise \end{Bmatrix} \tag{2.15}$$

The variation in viscosity as a function of radius in the dimensionless form is as follows:

$$\overline{\mu} = [1 + \tilde{\lambda}H(1 - \overline{r}^m)].$$

3. NUMERICAL SOLUTION OF THE PROBLEM

The finite difference approach with no-slip boundary condition is used to solve the nonlinear dimensionless partial differential equations. Second-order derivatives are discretised using the central difference scheme, whereas the forward difference scheme is used to discretise the first-order derivatives. Grids of size 0.025 are used to partition the blood flow zone, and at various grid positions, the governing equations are solved by increasing I in the radial direction. The tri-diagonal system of equations created by the finite difference equations found at each grid point is solved using the Thomas algorithm [55].

The discretised equations are as follows:

$$\left(\frac{\partial \mathrm{p}}{\partial z}\right)_{\mathrm{i,j}} = \frac{\left(\mu_{\mathrm{i,j}}\right)}{\mathrm{r_{i,j}}}\left(\frac{\mathrm{u_{i+1,j}} - \mathrm{u_{i,j}}}{\Delta \mathrm{r}}\right) + \left(\mu_{\mathrm{i,j}}\right)\frac{\mathrm{u_{i+1,j}} - 2\mathrm{u_{i,j}} + \mathrm{u_{i-1,j}}}{(\Delta \mathrm{r})^2} - \left(\frac{\left(\mu_{\mathrm{i,j}}\right)}{\mathrm{K}}\right)\mathrm{u_{i,j}} + \left(\frac{\mathrm{u_{i+1,j}} - \mathrm{u_{i,j}}}{\Delta \mathrm{r}}\right)\left(\frac{\mu_{\mathrm{i+1,j}} - \mu_{\mathrm{i,j}}}{\Delta \mathrm{r}}\right) + Gr\ cos\beta\ \theta_{i,j} + Cr\ cos\beta\ \theta_{i,j} - \mathrm{u}_{i,j}\ \frac{M^2}{1+Be^2} \tag{3.1}$$

$$\left(1+\frac{4}{3R}\right)\left(\frac{1}{\mathrm{r_{i,j}}}\frac{\theta_{\mathrm{i+1,j}} - \theta_{\mathrm{i,j}}}{\Delta \mathrm{r}} + \frac{\theta_{\mathrm{i+1,j}} - 2\theta_{\mathrm{i,j}} + \theta_{\mathrm{i-1,j}}}{(\Delta \mathrm{r})^2}\right) + Br\ \left(\mu_{\mathrm{i,j}}\right)\left(\left(\frac{\mathrm{u_{i+1,j}} - \mathrm{u_{i,j}}}{(\Delta \mathrm{r})^2}\right)^2\right) + \frac{\mathrm{M}^2 {\mathrm{u}_{i,j}}^2 Br}{1+Be^2} = 0 \tag{3.2}$$

$$\left(\frac{1}{\mathrm{r_{i,j}}}\frac{\sigma_{\mathrm{i+1,j}} - \sigma_{\mathrm{i,j}}}{\Delta \mathrm{r}} + \frac{\sigma_{\mathrm{i+1,j}} - 2\sigma_{\mathrm{i,j}} + \sigma_{\mathrm{i-1,j}}}{(\Delta \mathrm{r})^2}\right) - \mathrm{K}\sigma_{i,j} = 0 \tag{3.3}$$

The appropriate mesh size for the aforementioned calculation is $\Delta \mathrm{r} = 0.025$. The procedure is carried out iteratively till the error was less than 10^{-5}. When the error is less than or equal to 10^{-5}, the iterative process will stop. To derive the velocity, temperature and concentration profiles, these equations are initially solved without considering the linked factors. The final values for velocity, temperature and concentration are then calculated by repeatedly inserting the starting values that were acquired.

4. RESULTS AND DISCUSSION

This section describes the velocity, temperature and concentration profiles along the arterial radius and discusses the effects of hematocrit, Brinkman number, Hall parameter, porosity parameter, Grashof number, chemical reaction parameter, modified Grashof number, Brownian motion and thermophoresis parameter. Graphical representations of the effects using physical interpretation are used. Calculations are made for shear stress, rate of heat transfer (in terms of Nusselt number) and rate of mass transfer coefficient (in terms of Sherwood number). The consequences of mass and heat transport have also been covered. H = 0.1, Gr = 5, m = 2, K1 = 2, Cr = 2, Br = 7, R = 2, k = 2, M = 0.5, Z = 0.5, d = 0.25, = 0.05 and K = 2 are the default values for the constants.

4.1. Velocity profile

Variations in the velocity profile with hematocrit are shown in Fig. 2. Due to the red blood cells' increased contribution to viscosity, it is shown that velocity drops as hematocrit increases.

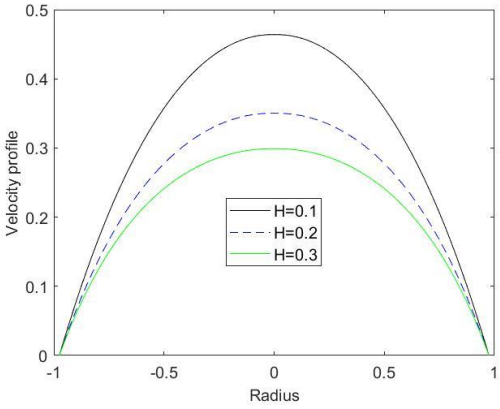

Fig. 2. Velocity profile with variation in hematocrit

In Fig. 3, the velocity is shown to decrease when the Hall parameter increased. This shows that the applied magnetic field decreases while the induced electric field increases. The effect of velocity fluctuation with the Brinkman number is shown in Figure 4. As seen in Fig. 4, it is observed that velocity rises as the Brinkman number rises. The rise in viscous dissipation, which in turn causes the velocity to rise, contributes to the rise in the Brinkman number. Since viscous dissipation provides internal energy to the flow, it strongly affects the spatial organisation of temperatures. The effect of viscous dissipation, brought about by shear stress inside the fluid layer, is responsible for the rise in the

DOI 10.2478/ama-2024-0017

Brinkman number. The variation in velocity with the Grashof number is shown in Fig.5, which shows that velocity increases with the Grashof number. The Grashof number signifies the ratio of thermal resistive force to viscous force. With an increase in the Grashof number, the viscous force decreases, causing the flow velocity to increase.

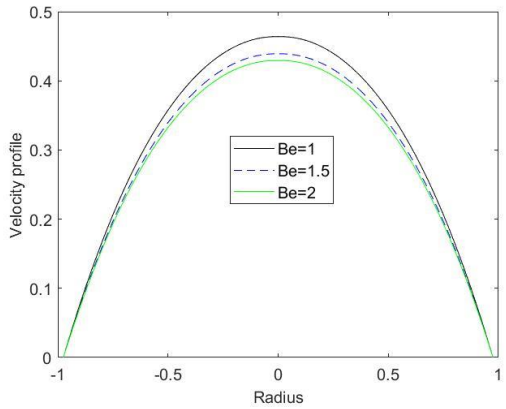

Fig. 3. Velocity profile with variation in Hall parameter

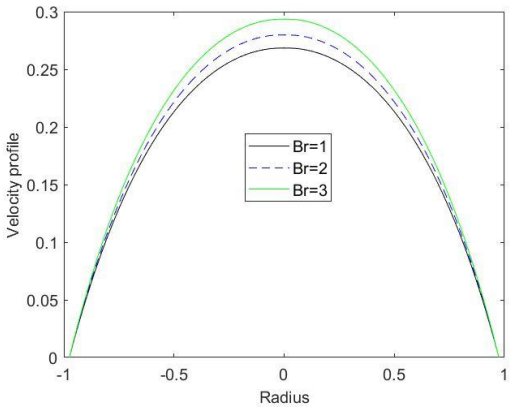

Fig. 4. Velocity profile with variation in Brinkman number

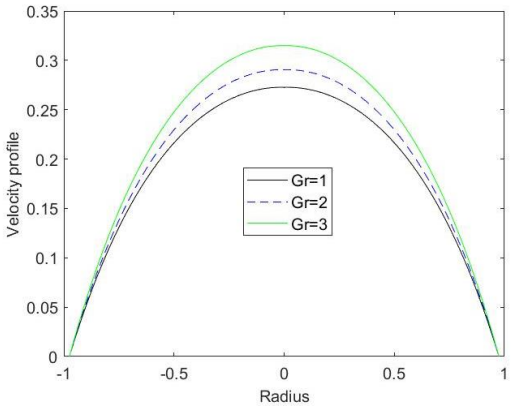

Fig. 5. Velocity profile with variation in Grashof number

The effect of the modified Grashof number on variation in velocity is shown in Fig. 6. It is noted that velocity increases with a decrease in the modified Grashof number, as viscosity decreases with an increase in velocity. Variation in velocity with porosity parameter is determined in Fig. 7. Figure 7 illustrates how porosity causes an increase in void volume, which causes velocity to increase. The thickness of the momentum boundary layer enhances as the parameter K1 rises. When the porosity of the medium increases, as measured by a bigger value of K1, the fluid gets more spacious and thus, enhance the fluid velocity. Figure 8 illustrates how velocity varies with the angle of inclination. According to Fig. 8, velocity decreases as the angle of inclination increases. Thermal diffusion causes this change in velocity profile, which lessens the impact of buoyancy on the fluid.

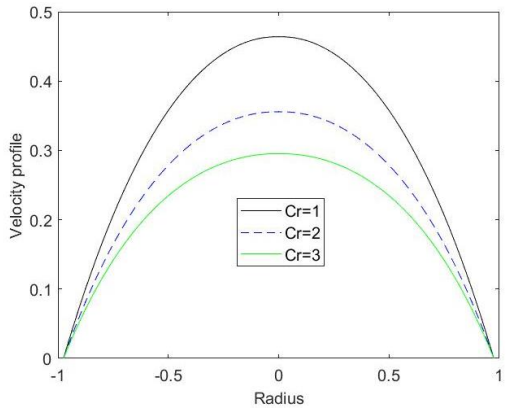

Fig. 6. Velocity profile with variation in modified Grashof number

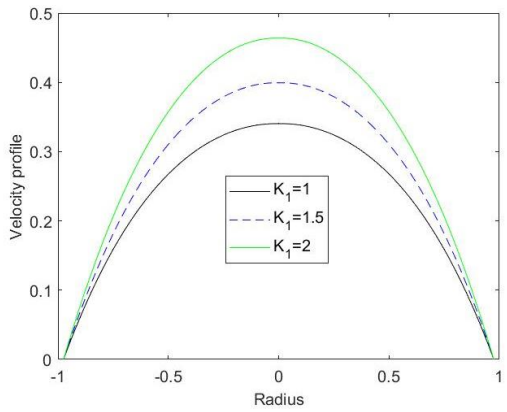

Fig. 7. Velocity profile with variation in porosity parameter

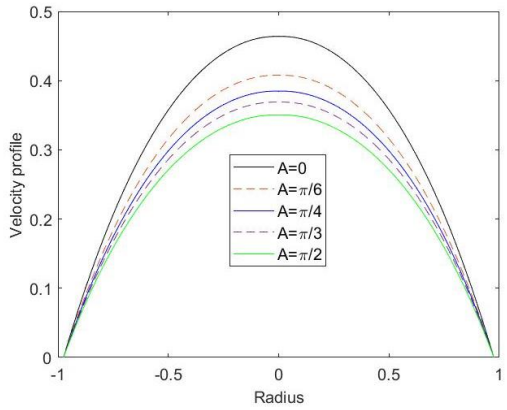

Fig. 8. Velocity profile with variation in angle of inclination

4.2. Temperature profile

Figure 9 illustrates how temperature changes in relation to hematocrit. Due to an increase in viscosity, it is evident that temperature drops as hematocrit increases. The impact of the Hall

parameter on the temperature profile is shown in Fig. 10. In Fig. 10, it is seen that temperature drops as the Hall parameter rises. Physically, the temperature falls as the velocity lowers with the Lorentz force and viscous dissipation reduces. This trend is also found in a previous study [56].

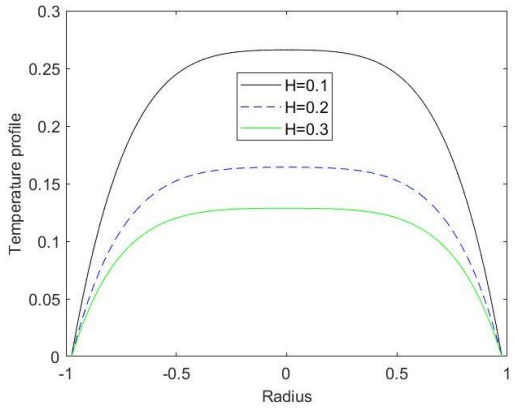

Fig. 9. Temperature profile with variation in hematocrit

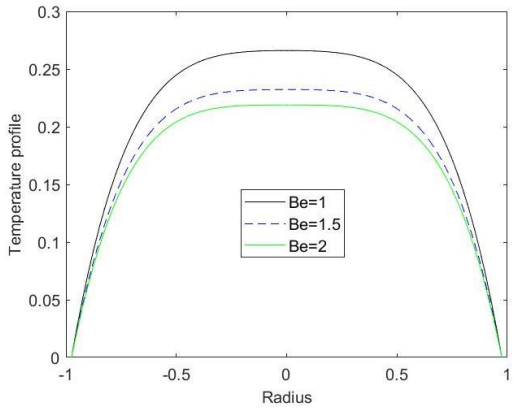

Fig. 10. Temperature profile with variation in Hall parameter

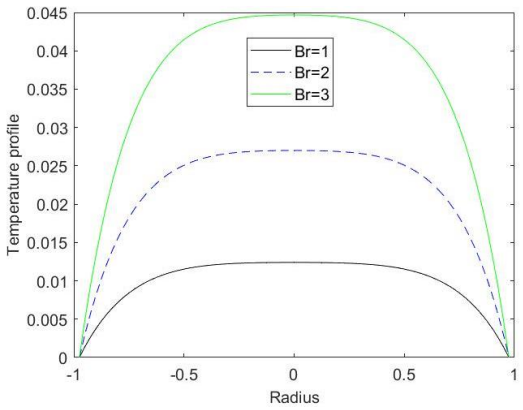

Fig. 11. Temperature profile with variation in Brinkman number

Fig. 11 shows the relationship between temperature variation and the Brinkman number. Due to an increase in viscous dissipation, temperature rises as the Brinkman number rises.

In Fig. 12, the temperature rises as the amount of heat from radiation increases. The fluid produces heat, which thickens the thermal boundary layer as the radiation parameter rises. Thus, fluid temperature increases with an increase in R. A possible explanation for the rising trend in the temperature profile is the generation of additional thermal energy. So, this shows that the radiation parameter R is essential in the process of modifying the temperature profile. The effect of inclination angle on the temperature profile is shown in Fig.13. Temperature decreases with an increase in the angle of inclination, as observed in Fig.13.

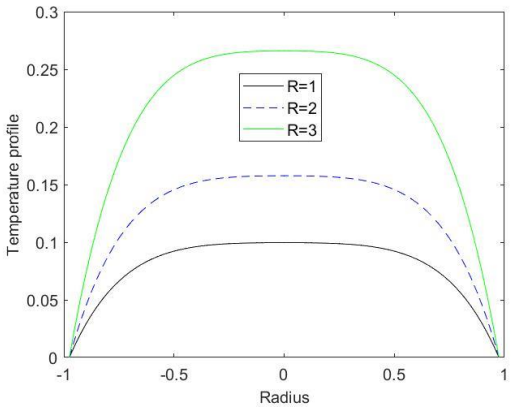

Fig. 12. Temperature profile with variation in radiation parameter

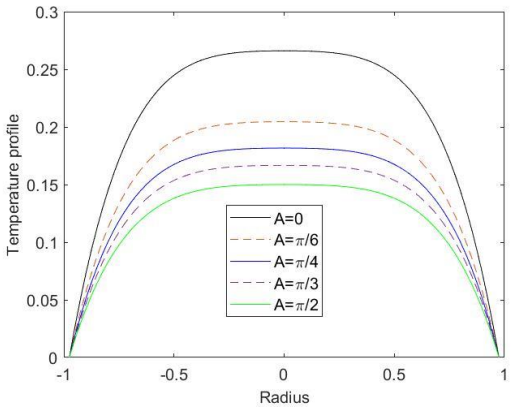

Fig. 13. Temperature profile with variation in angle of inclination

4.3. Concentration profile

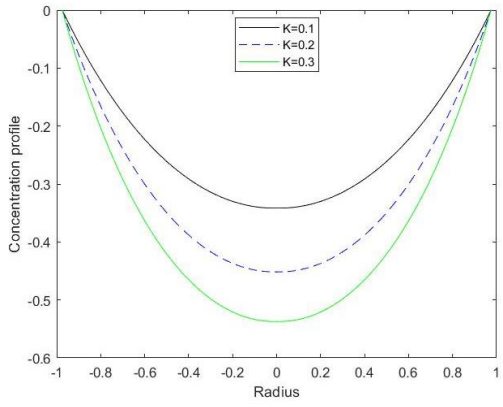

Fig. 14. Concentration profile with variation in chemical reaction parameter

Variation in concentration with chemical reaction parameter is depicted in Fig. 14. As noticed in Fig. 14, concentration rises as

the chemical reaction parameter decreases due to a drop in temperature. The rise in solute molecules that results from an increase in the chemical reaction parameter reduces the thickness of the concentration boundary layer.

4.4. Shear stress vs stenosis height

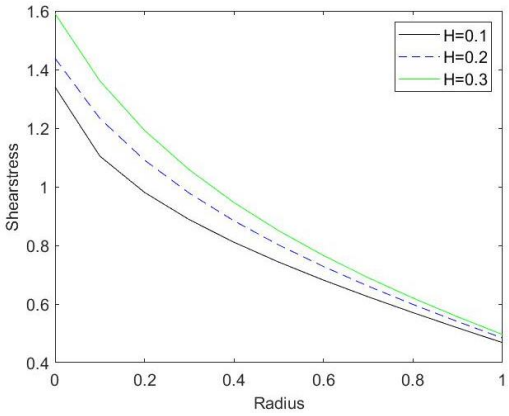

Fig. 15. Shear stress profile with variation in hematocrit

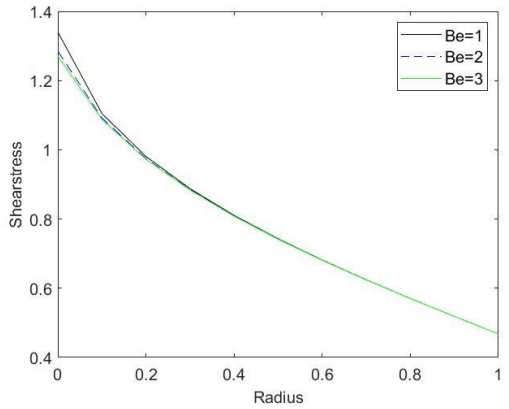

Fig. 16. Shear stress profile with variation in Hall parameter

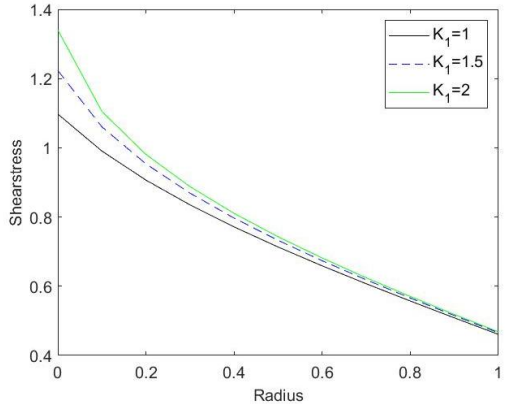

Fig. 17. Shear stress profile with variation in porosity parameter

Fig.15 displays the effect of hematocrit on shear stress. It is noted the figure that as viscosity rises, there is an increase in shear stress together with a rise in hematocrit. With an increase in stenosis height, shear stress reduces. According to Fig. 16, shear stress reduces as the Hall parameter rises. Due to the increase in velocity in Fig. 17, shear stress increases with the porosity parameter. Fig. 18 shows the variation in shear stress with the angle of inclination. As seen in the figure, shear stress reduces as the angle of inclination increases.

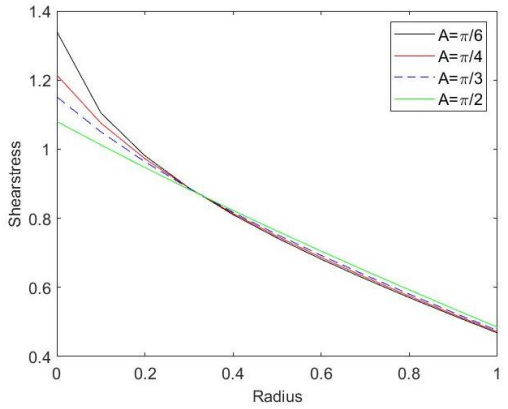

Fig. 18. Shear stress profile with variation in angle of inclination

4.5. Nusselt number vs stenosis neight

Fig. 19 shows the variation in the Nusselt number with hematocrit parameter. The Nusselt number decreases with an increase in hematocrit, as shown in the figure. This indicates that with the rise in hematocrit, conductive heat transfer increases. Variation in the Nusselt number with Hall parameter is represented in Fig. 20. The Nusselt number falls as Hall parameter increases, indicating that heat transfer decreases as electromagnetic force increases.

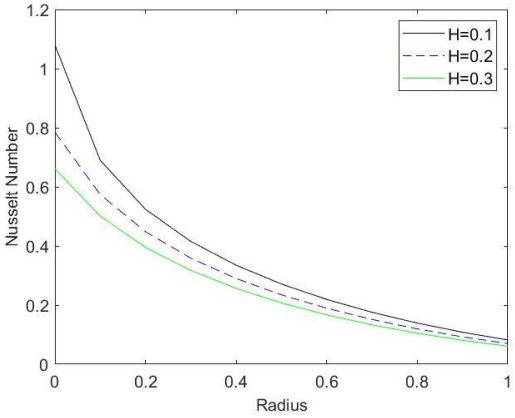

Fig.19. Nusselt number profile with variation in haematocrit

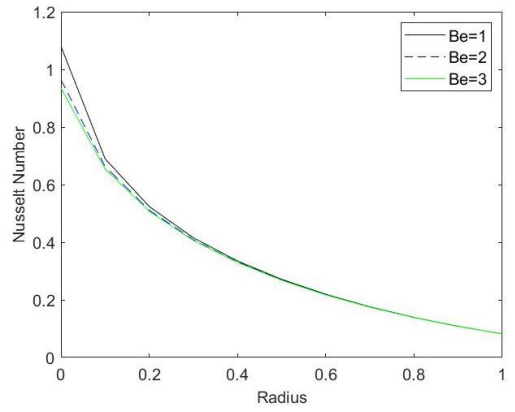

Fig. 20. Nusselt number profile with variation in Hall parameter

Fig. 21 shows a variation in the Nusselt number with the Brinkman number. According to Fig. 21, the Nusselt number rises when Brinkman increases, as also observed in a previous study [57]. In Fig. 22, it is noted that the Nusselt number rises when the radiation parameter rises because of an increase in heat transfer at higher temperatures. A similar trend can be observed in the study by AlBaidani et al. [58]. Figure 23 shows how the Nusselt number varies with the angle of inclination. In Fig. 23, it can be seen that the Nusselt number drops as the angle of inclination increases.

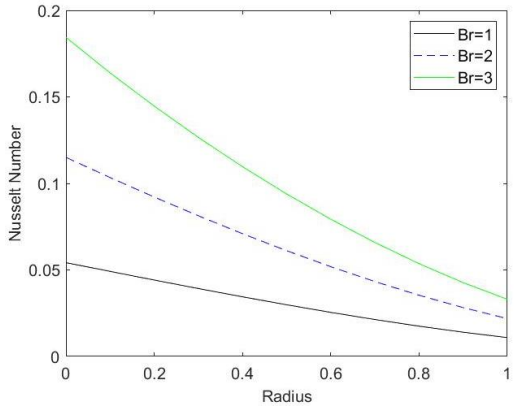

Fig. 21. Nusselt number profile with variation in Brinkman number

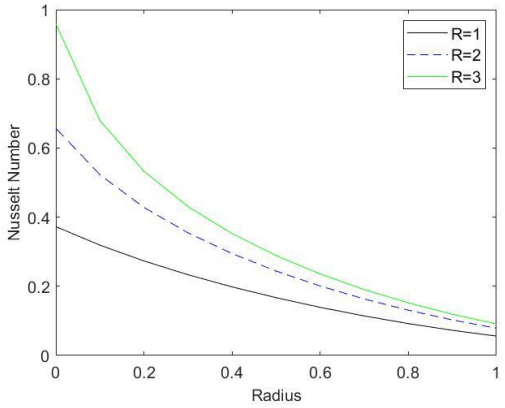

Fig. 22. Nusselt number profile with variation in radiation parameter

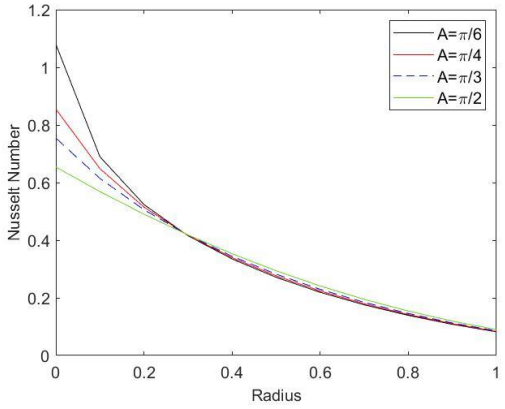

Fig. 23. Nusselt number profile with variation in angle of inclination

4.6. Variation in sherwood number

Fig. 24 displays the Sherwood number variation with respect to the chemical reaction parameter. Until a stenosis height of 0.1, it is seen that the Sherwood number drops with an increase in chemical reaction parameter; after that, a reverse tendency is seen, which is also noted in a previous study [59].

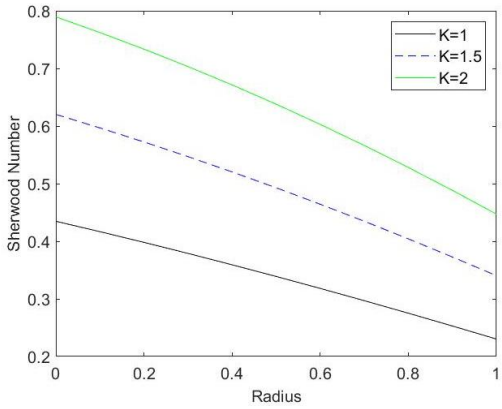

Fig. 24. Variation in Sherwood number profile with variation in chemical reaction parameter

5. CONCLUSION

The hemodynamic properties of blood flow are examined in the current study in the presence of the Hall effect. Using the finite difference method, the mathematical blood flow model through composite stenosis is analysed. The flow is subjected to radiation, and copper-suspended nanofluid has been considered. Due to the presence of haemoglobin, white blood cells, platelets, etc., the blood is not homogeneous; as a result, its viscosity varies. Consideration has been given to the Einstein viscosity model to investigate the effects of altering viscosity. The current study provides insights into the non-surgical management of stenosis and other defects while minimising post-operative complications. Key findings of the analysis as follows:

As the Hartman number increases, the velocity drops. This is as a result of the Lorentz force that the applied magnetic field has generated. Blood flow in the arteries is resisted by the Lorentz force.

The velocity drops as the Hall parameter rises, indicating a rise in the induced electric field brought on by the applied magnetic field.

There is an increase in viscous dissipation near the boundary, which leads to an increase in velocity, due to the Brinkman number effect on velocity.

As the Hall parameter increases, the temperature drops. This is brought on by a decline in velocity, which also results in a decline in viscous dissipation.

As the Hartman number rises, the temperature falls, suggesting that the viscous force is reduced as electromagnetic forces rise.

As the Hall parameter increases due to a reduction in velocity, the shear stress decreases.

As viscous dissipation rises, shear stress rises with the Brinkman number.

With an increase in conductive heat transfer with viscous dissipation, the Nusselt number rises with the Brinkman number.

Nomenclature:

u – Velocity in the z-direction
v - Velocity in the r-direction
R(z) - Radius of the artery in the obstructed region
R_0 - radius of the normal artery
ρ_f - Effective density of the nanofluid
α_T - Coefficient of volume expansion with temperature
α_c - Volumetric coefficient of expansion with concentration
C_{pf} - Specific heat of the fluid at constant pressure
σ - Electrical conductivity
T_m - Mean fluid temperature
D_m - Coefficient of mass diffusivity
K_T - Thermal diffusion ratio
k_T - Thermal conductivity of the fluid
μ - Viscosity
Pr - Prandtl number
Ec - Eckert number
Sr - Soret number
Sc - Schmidt number
ω – Viscosity parameter
Gr - Grashof number
Cr - local concentration number
Df - Dufour number
Br – Brinkman number

REFERENCES:

1. Nadeem S, Ijaz S. Theoretical analysis of metallic nanoparticles on blood flow through stenosed artery with permeable walls. Physics Letters A. 2015; 379(6): 542-554.
2. Liepsch D, Singh M, Lee M. Experimental analysis of the influence of stenotic geometry on steady flow. Biorheology.1991, 29(4): 419-431.
3. Ellahi R, Rahman SU, Nadeem S, Akbar N S. Blood flow of nanofluid through an artery with composite stenosis and permeable walls. Applied Nanoscience. 2014; 4(8): 919-926.
4. Bali R, Awasthi U. A Casson fluid model for multiple stenosed artery in the presence of magnetic field. Applied Mathematics. 2012; 3 (5): 436-441.
5. Nadeem S, Jaz S, Akbar NS. Nanoparticle analysis for blood flow of Prandtl fluid model with stenosis. International Nano Letters. 2013; 3(1): 1-13.
6. Késmárky G et al. Plasma viscosity: a forgotten variable. Clinical hemorheology and microcirculation. 2008; 39(1): 243-246.
7. Srivastava N. Analysis of flow characteristics of the blood flowing through an inclined tapered porous artery with mild stenosis under the influence of an inclined magnetic field. Journal of Biophysics. 2014; Article ID 797142,:1-9.
8. Baskurt K, Meiselman HJ. Blood rheology and hemodynamics. in Seminars in thrombosis and hemostasis. New York: Stratton Intercontinental Medical Book Corporation. c1974, 2003.
9. Lenz C et al. Blood viscosity modulates tissue perfusion–sometimes and somewhere. Transfusion Alternatives in Transfusion Medicine. 2007; 9(4): 265-272.
10. Kwon O et al. Effect of blood viscosity on oxygen transport in residual stenosed artery following angioplasty. Journal of biomechanical engineering. 2008; 130(1): 011003.
11. Asghar Z, Waqas M, Gondal M A, Khan W A. Electro-osmotically driven generalized Newtonian blood flow in a divergent micro-channel, Alexandria Engineering Journal. 2022; 61 (6), 4519-4528. https://doi.org/10.1016/j.aej.2021.10.012
12. Chen II, Sana S. Analysis of an intensive magnetic field on blood flow: part 2. Electromagnetic Biology and Medicine.1985; 4(1): 55-62.
13. Bose S et al. Lagrangian magnetic particle tracking through stenosed artery under pulsatile flow condition. Journal of Nanotechnology in Engineering and Medicine. 2013; 4(3): 031006.
14. Lübbe AS, Alexiou C, Bergemann C. Clinical applications of magnetic drug targeting. Journal of Surgical Research. 2001; 95(2): 200-206.
15. Sharma B K, Kumawat C, Makinde O D. Hemodynamical analysis of MHD two phase blood flow through a curved permeable artery having variable viscosity with heat and mass transfer, Biomechanics and Modeling in Mechanobiology.2022; 21(3): 797-825.
16. Kumawat C, Sharma B K, Al-Mdallal Qasem M, Gorji M M. Entropy generation for MHD two phase blood flow through a curved permeable artery having variable viscosity with heat and mass transfer. International Communications in Heat and Mass Transfer. 2022; 133: 105954.
17. Osalusi E, Side J, Harris R, Johnston B. On the effectiveness of viscous dissipation and Joule heating on steady MHD flow and heat transfer of a Bingham fluid over a porous rotating disk in the presence of Hall and ion-slip currents, International Communications in Heat and Mass Transfer. 2007; 34(9-10): 1030-1040,
18. Sharma B K, Jha A K, Chaudhary R C. Hall effect on MHD free convective flow of a viscous fluid past an infinite vertical porous plate with Heat source/sink effect. Romania Journal in Physics. 2007; 52(5-6): 487-504.
19. Sharma B K, Chaudhary R C. Hydromagnetic unsteady mixed convection and mass transfer flow past a vertical porous plate immersed in a porous medium with Hall effect. Engineering Transactions. 2008; 56(1): 3-23.
20. Mishra A, Sharma B K. MHD mixed convection flow in a rotating channel in the presence of an inclined magnetic field with the Hall effect. J. Eng. Phys. & Thermo Phy. 2017; 90(6): 1563-1574.
21. AlBaidani M M, Mishra NK, Alam MM, Eldin SM, AL-Zahrani AA Akgul A. Numerical analysis of magneto-radiated annular fin natural-convective heat transfer performance using advanced ternary nanofluid considering shape factors with heating source. Case Studies in Thermal Engineering. 2023; 44: 102825.
22. Ramzan M, Gul H, Chung J D, Kadry S, Chu Y M. Significance of Hall effect and ion slip in a three-dimensional bioconvective tangent hyperbolic nanouid flow subject to Arrhenius activation energy. Scientific Reports. 2020; 10(1): 1-15.
23. Das S, B Barman, Jana R N, Makinde O D. Hall and ion slip currents impact on electromagnetic blood flow conveying hybrid nanoparticles through an endoscope with peristaltic waves. BioNanoScience. 2021; 11(3): 770-792.
24. Raja MA, Shoaib M, Hussain S, Nisar KS, Islam S. Computational intelligence of Levenberg-Marquardt backpropagation neural networks to study thermal radiation and Hall effects on boundary layer flow past a stretching sheet. Int Commun Heat Mass Transf. 2022; 130: 105799.
25. Das M, Nandi S, Kumbhakar B. Hall effect on unsteady MHD 3D Carreau nanofluid flow past a stretching sheet with Navier's slip and nonlinear thermal radiation. PJMs. 2022: 11.
26. Kada B, Pasha A A, Asghar Z, Khan M W S, Aris I B, Shaikh M S. Carreau–Yasuda fluid flow generated via metachronal waves of cilia in a micro-channel. Physics of Fluids. 2023; 35(1):013110. https://doi.org/10.1063/5.0134777
27. Asghar Z, Shah RA, Ali N. A numerical framework for modeling the dynamics of micro-organism movement on Carreau-Yasuda layer. Soft Comput. 2023; 27: 8525–8539. https://doi.org/10.1007/s00500-023-08236-3
28. Virmani R et al. Pathology of radiation-induced coronary artery disease in human and pig. Cardiovascular radiation medicine. 1999; 1(1): 98-101.
29. Bejawada S , Nandeppanavar M M. Effect of thermal radiation on magnetohydrodynamics heat transfer micropolar fluid flow over a vertical moving porous plate. Exp. Comput. Multiph. Flow 2023;5: 149–158. https://doi.org/10.1007/s42757-021-0131-5

30. Jamshed W, Ramesh GK, Roopa GS, Nisar KS, Safdar R, Madhukesh JK, Shahzad F, Isa SSPM, Goud BS, Eid MR. Electromagnetic radiation and convective slippery stipulation influence in viscous second grade nanofluid through penetrable material. Z Angew Math Mech. 2022; 202200002. https://doi.org/10.1002/zamm.202200002
31. Reddy Y D, Goud B S . Comprehensive analysis of thermal radiation impact on an unsteady MHD nanofluid flow across an infinite vertical flat plate with ramped temperature with heat consumption. Results in Engineering. 2022; 17: 100796. https://doi.org/10.1016/j.rineng.2022.100796
32. Sharma, B K, Yadav K, Mishra N K, Chaudhary R C. Soret and Dufour effects on unsteady MHD mixed convection flow past a radiative vertical porous plate embedded in a porous medium with chemical reaction. Applied Mathematics. 2012; 3(7): 717-723.
33. Sharma B K, Gupta S, Krishna V V, Bhargavi R J. Soret and Dufour effects on an unsteady MHD mixed convective flow past an infinite vertical plate with Ohmic dissipation and heat source. Afrika Matematika. 2014; 25 (3): 799-825.
34. Makinde OD, Reddy G M, Reddy K V. Effects of thermal radiation on MHD peristaltic motion of walters-b fluid with heat source and slip conditions. Journal of Applied Fluid Mechanics. 2017; 10(4): 1105-1112.
35. Mishra NK. Computational analysis of Soret and Dufour effects on nanofluid flow through a stenosed artery in the presence of temperature-dependent viscosity. Acta Mechanica et Automatica. 2023;17(2): 246-253.
36. Taylor R et al. Small particles, big impacts: a review of the diverse applications of nanofluids. Journal of Applied Physics. 2013; 113(1): 011301.
37. Su X, Zheng L. Hall effect on MHD flow and heat transfer of nanofluids over a stretching wedge in the presence of velocity slip and Joule heating. Central European Journal of Physics. 2013; 11(12): 1694-1703.
38. Gandhi R, Sharma B K, Kumawat C, Bég O A. Modeling and analysis of magnetic hybrid nanoparticle(Au-Al2O3/blood) based drug delivery through a bell-shaped occluded artery with Joule heating, viscous dissipation and variable viscosity effects, Proceedings of the Institution of Mechanical Engineers. Part E: Journal of Process Mechanical Engineering. 2022; 236(5): 2024-2043.
39. Sharma B K, Gandhi Rishu, Bhatti M M. Entropy analysis of thermally radiating MHD slip flow of hybrid nanoparticles (Au-Al2O3/Blood) through a tapered multi-stenosed artery. Chemical Physics Letters. 2022; 790: 139348.
40. Asghar Z, Shah RA, Shatanawi W et al. A theoretical approach to mathematical modeling of sperm swimming in viscoelastic Ellis fluid in a passive canal. Arch Appl Mech. 2023; 93: 1525–1534. https://doi.org/10.1007/s00419-022-02343-7
41. Asghar Z, Elmoasry A, Shatanawi W, Gondal M A. An exact solution for directional cell movement over Jeffrey slime layer with surface roughness effects, Physics of Fluids. 2023; 35: 041901. https://doi.org/10.1063/5.0143053
42. Asghar Z; Khan Muhammad W S, Shatanawi W, Gondal M A, Ghaffari A. An IFDM analysis of low Reynolds number flow generated in a complex wavy curved passage formed by artificial beating cilia. International Journal of Modern Physics B. 2023; 37 (19): 2350187. https://doi.org/10.1142/S0217979223501874
43. Asghar Z. Enhancing motility of micro-swimmers via electric and dynamical interaction effects. Eur. Phys. J. Plus. 2023; 138: 357. https://doi.org/10.1140/epjp/s13360-023-03963-w
44. Goud B. S, Nandeppanavar M M. Chemical Reaction and Mhd Flow for Magnetic Field Effect on Heat and Mass Transfer of Fluid Flow Through a Porous Medium Onto a Moving Vertical Plate. International Journal of Applied Mechanics and Engineering. 2022; 27 (2):226-244. https://doi.org/10.2478/ijame-2022-0030
45. Sharma BK, Sharma P, Mishra NK, Noeiaghdam S, Fernandez-Gamiz U. Bayesian regularization networks for micropolar ternary hybrid nanofluid flow of blood with homogeneous and heterogeneous reactions: Entropy generation optimization. Alexandria Engineering Journal. 2023;77:127-148.
46. Goud B S, Srilatha P, Srinivasulu T, Reddy Y D, Kanti Sandeep Kumar K S. Induced by heat source on unsteady MHD free convective flow of Casson fluid past a vertically oscillating plate through porous medium utilizing finite difference method, Materials Today: Proceedings 2023. https://doi.org/10.1016/j.matpr.2023.01.378.
47. Sharma BK, Sharma P, Mishra NK, Fernandez-Gamiz U. Darcy-Forchheimer hybrid nanofluid flow over the rotating Riga disk in the presence of chemical reaction: Artificial neural network approach. Alexandria Engineering Journal. 2023; 76:101-130. https://doi.org/10.1016/j.aej.2023.06.014
48. Asogwa K K, Goud B S. Impact of velocity slip and heat source on tangent hyperbolic nanofluid flow over an electromagnetic surface with Soret effect and variable suction/injection. Proceedings of the Institution of Mechanical Engineers. Part E: Journal of Process Mechanical Engineering. 2023; 237(3):645-657. doi:10.1177/09544089221106662
49. Sharma B K, Gandhi R, Mishra N K, Al-Mdallal Q. Entropy generation minimization of higher-order endothermic/exothermic chemical reaction with activation energy on MHD mixed convective flow over a stretching surface. Scientific Reports. 2022; 12: 17688. https://doi.org/10.1038/s41598-022-22521-5
50. Srinivasulu T, Goud B S. Effect of inclined magnetic field on flow, heat and mass transfer of Williamson nanofluid over a stretching sheet. Case Studies in Thermal Engineering. 2021; 23: 100819. https://doi.org/10.1016/j.csite.2020.100819
51. Chakravarty S, Mandal P. Mathematical modelling of blood flow through an overlapping arterial stenosis. Mathematical and computer modelling. 1994; 19(1): 59-70.
52. Chakravarty S, Mandal P. A nonlinear two-dimensional model of blood flow in an overlapping arterial stenosis subjected to body acceleration. Mathematical and computer modelling. 1996; 24(1): 43-58.
53. Ellahi R, Rahman SU, Nadeem S. Blood flow of Jeffrey fluid in a catherized tapered artery with the suspension of nanoparticles. Physics Letters A. 2014; 378: 2973–2980.
54. Lih MMS. Transport phenomena in medicine and biology. Biomedical engineering and health systems. 1975. Wiley.
55. Datta BN. Numerical linear algebra and applications 2012. SIAM.
56. Khanduri U, Sharma B K. Mathematical analysis of Hall effect and hematocrit dependent viscosity on Au/Go-blood hybrid nanofluid flow through a stenosed catheterized artery with thrombosis. In Advances in Mathematical Modelling. Applied Analysis and Computation: Proceedings of ICMMAAC 2022: 121-137. Cham: Springer Nature Switzerland.
57. Sharma BK, Kumar A, Gandhi R, Bhatti MM, Mishra NK. Entropy generation and thermal radiation analysis of EMHD Jeffrey nanofluid flow: Applications in solar energy. Nanomaterials. 2023; 13(3): 544.
58. AlBaidani MM, Mishra NK, Ahmad Z, Eldin SM, Haq EU. Numerical study of thermal enhancement in ZnO-SAE50 nanolubricant over a spherical magnetized surface influenced by Newtonian heating and thermal radiation. Case Studies in Thermal Engineering. 2023; 45: 102917.
59. Sharma PK, Sharma BK, Mishra N K, Rajesh H. Impact of Arrhenius activation energy on MHD nanofluid flow past a stretching sheet with exponential heat source: A modified Buongiorno's model approach. International Journal of Modern Physics B. 2023; 2350284. 10.1142/S0217979223502843.

Nidhish Kumar Mishra: https://orcid.org/0000-0003-4502-261X